Genetic Mouse Models of Autism Spectrum Disorder Present Subtle Heterogenous Cardiac Abnormalities

*Stephania Assimopoulos[1,2,3], Christopher Hammill[1,2], Darren J. Fernandes[1,2], Tara Leigh Spencer Noakes[1,2], Yu-Qing Zhou[1], Lauryl M. J. Nutter[2,4], Jacob Ellegood[1,2], Evdokia Anagnostou[5], John G. Sled[1,2,3], Jason P. Lerch[1,2,3,6]

*Corresponding Author

Affiliations:

1. Mouse Imaging Centre, Hospital for Sick Children, Toronto, Ontario, Canada
2. The Hospital for Sick Children, Toronto, Ontario, Canada
3. Department of Medical Biophysics, University of Toronto, Toronto, Ontario, Canada
4. The Centre for Phenogenomics, Toronto, Ontario, Canada
5. Holland Bloorview Kids Rehabilitation Hospital, Toronto, Ontario Canada
6. Wellcome Centre for Integrative Neuroimaging, The University of Oxford, Oxford, UK

Abstract

Background: Autism Spectrum Disorder (ASD) and Congenital Heart Disease (CHD) are strongly linked on a functional and genetic level. Most work has been focused on the neurodevelopmental abnormalities in CHD, whereas the investigation of cardiac abnormalities (CHD or not) in ASD has been more limited. In this work we investigate the prevalence of cardiac comorbidities relative to genetic contributors of ASD.

Methods: Using high frequency ultrasound imaging, we screened 9 mouse models with ASD-related genetic alterations (*Arid1b*$^{(+/-)}$, *Chd8*$^{(+/-)}$, 16p11.2 (deletion), *Sgsh*$^{(+/-)}$, *Sgsh*$^{(-/-)}$, *Shank3 Δexon 4-9*$^{(+/-)}$, *Shank3 Δexon 4-9*$^{(-/-)}$, *Fmr1*$^{(-/-)}$, *Vps13b*$^{(+/-)}$), along with pooled wild-type littermates (WT). Using a standardised imaging protocol, the cardiac morphological and functional parameters measured were thickness and thickening of the left-ventricular (LV) anterior and posterior walls, LV chamber diameter, LV fractional shortening, heart rate (HR), aorta diameter (AoD), LV stroke volume and cardiac output.

Results: Small-scale alterations in cardiac structure and function were found in the mutant groups compared to WTs. When mutant groups were compared to each other, a greater number of significant differences was observed than when mutant groups were compared to WT controls. Mutant groups differed primarily in measures of structure (LV chamber diameter and anterior wall thickness, HR, AoD), while when compared to WT controls, they differed in both structure and function (LV anterior wall thickness and thickening, LV chamber diameter and fractional shortening, HR). The mutant groups with most differences to WT controls are 16p11.2 (deletion), *Fmr*$^{(-/-)}$, *Arid1b*$^{(+/-)}$. Among mutant groups, the groups differing most from the others were 16p11.2 (deletion), *Sgsh*$^{(+/-)}$, *Fmr1*$^{(-/-)}$.

Our results recapitulate the clinical findings associated with each genetic mutation and broadly with ASD, to the extent that a direct comparison is possible. Additionally, our protocol was verified as an effective screening protocol capturing various dimensions of cardiac function.

Conclusions: The characteristic heterogeneity of ASD was recapitulated in the cardiac phenotype of ASD-models. However, determining whether certain mutant groups differ in morphological or functional measures (as a general category) can offer insight regarding common underlying mechanisms. Clinically, knowledge of cardiac abnormalities in ASD can be essential as even non-lethal cardiac abnormalities can impact normal development.

Keywords: autism, cardiac phenotype/cardiology, comorbidities, genetic mouse models, phenotyping, ultrasound biomicroscopy

Background

Autism Spectrum Disorder (ASD) and Congenital Heart Disease (CHD) have been found to be strongly linked both on a functional (1–3) and a genetic level (4–6). ASD is a neurodevelopmental disorder (NDD) with an occurrence rate >1%, highly heterogeneous in etiology and phenotype (7,8). It is primarily associated with behavioural deficits, but also has associated comorbidities, amongst which cardiac are common (9). CHD is the most common birth defect (10) present in 0.8%-1.2% of all live births worldwide (11). It accounts for about 3% of infant deaths and, of those, 46% are due to congenital malformations (12). Neurodevelopmental differences, including language, motor, cognitive and social deficits, occur in 10% of children with congenital heart disease and in 50% of those with severe congenital heart disease (13).

The primary focus of the investigation in the NDD-CHD association, has been to identify the frequency of neurodevelopmental differences in various CHD cases. There are only a few studies on the ASD-CHD association, and they report an increased risk of ASD in CHD (6,14). In CHD, brain development is found to be atypical on MRI studies, where newborns with CHD were found to have smaller for gestational age total brain volume, reduced metabolism and delayed cortical development and folding compared to controls (following age and weight adjustment) (1,15–18), both prior to and following the necessary corrective cardiac surgeries (1,18). Moreover, known risk factors can only account for 30% of the neurodevelopmental outcome following such interventions, suggesting there are other genetic and epigenetic factors contributing to the outcomes (19). Reinforcing the association between cardiac and brain development on the genetic level, a large study performing exome sequencing on 1,213 congenital heart disease parent-offspring trios identified 69 genes containing damaging *de novo*

mutations known to be associated with both ASD and NDD, all of which are in the top quartile of both developmental heart and brain expression (far more than expected by chance), thus revealing a shared genetic contribution to congenital heart disease and NDD (4).

Contrary to the aforementioned work on NDDs in CHD, the investigation of cardiac abnormalities in ASD, whether specifically CHD or not, has been more limited. The incidence rate of cardiac abnormalities reported in ASD varies in the literature depending on the cardiac abnormalities considered and the age of the subjects. In an adult U.S.A. population sample, Croen et al. (2015) considered three categories of cardiovascular diseases (dyslipidemia, hypertension and all other) and reported a joint prevalence of 36.96% and an odds ratio of 2.54, with hypertension being the most prevalent amongst the three groups (20). Similarly, in an adult French population subset, Miot et al. (2019) considered five categories of which three were significant (heart failure, orthostatic hypotension, peripheral vascular disease) and reported a joint prevalence of 15.37%, while separately considering hypertension with a prevalence of 13.56% (21). A population study in Western Australia assessing the occurrence rate of birth defects diagnosed before the age of 6 in children with ASD, reported a 1.3% incidence rate with a 1.2 odds ratio for cardiovascular system defects (22).

ASD is associated with a vast spectrum of cardiac abnormalities, including morphological alterations, cardiac dysrhythmias (ventricular flutter, fibrillation, and premature beats) and dysregulated resting autonomic activity. Autonomic dysregulation is one of the main abnormalities observed in syndromic cases of ASD (5,23). Specifically, cardiac dysrhythmias and various morphological defects are most prominent in chromosomal disorders of 22q11 deletion syndrome (DiGeorge, velocardiofacial syndrome) (24,25), in which the co-existence of a cardiac abnormality has been found to also result in reduced cortical and hippocampal volume

(26). Additionally, cardiac arrythmias are commonly seen in patients with Timothy syndrome (*CACNA1C* mutation) (27,28). Similarly, CHARGE syndrome, a genetic disorder manifested through a non-random association of congenital anomalies (29), has a known associated cardiac dysfunction (30–32). Related investigations have been conducted for other NDDs, such as Trisomy21 (Down Syndrome) and Turner Syndrome, in which congenital heart disease is present in 50% and 30% respectively (23,33), as well as in Rett syndrome (34). Dysregulation in resting autonomic activity, or equivalently vagus nerve activity, is also observed in non-syndromic cases of ASD. Specifically, sympathetic overarousal, parasympathetic underactivity or atypical interaction between the two have been observed (35–37). Such dysregulation has been seen in both children and adults with ASD and is mainly manifested as reduced resting-state heart rate (HR) variability, slowed respiratory sinus arrythmia (RSA) and/or increased HR (36–38). Dysregulation in autonomic activity/vagus nerve function can generally lead to various cardiovascular complications thus warranting further investigation. Reports of morphological cardiac abnormalities have been sparse and mainly reported in syndromes associated with ASD, such as Tuberous Sclerosis (*TSC1* or *TSC2*) and Fragile X syndrome (5,23,39,40). Finally, accumulating evidence suggests that severe cardiac abnormalities do not simply co-occur with NDDs but may also contribute to the observed neurodevelopmental abnormalities (1,19,25), thus further highlighting the need for deeper investigation of cardiac abnormalities in ASD.

It is apparent that cardiac comorbidities in ASD may arise as a result of various, potentially coinciding, factors. In this work we investigate the prevalence of cardiac comorbidities relative to prominent genetic contributors of ASD. Specifically, using high frequency ultrasound imaging, we screen a set of ASD-related genetic mouse models with a standardised protocol to assess the incidence of cardiac abnormalities.

This study is performed in mice to allow for tightly controlled genetics, environment and experimental procedures. Studies in mouse models of ASD have been useful in determining the impact of genomic variation on brain differences across species (41). In addition, the development of the healthy mouse heart is comparable to that of humans and various mouse models of CHD have been reported to adequately replicate the corresponding human condition (42), suggesting that mouse models may be well suited for this endeavour.

Methods

Animals:

Adult (60 days old +/- 1 day) male mice from 9 mouse models of 7 ASD-related genes (Table 1) were used in this study. The abnormalities and their effects, resulting from the underlying genetic mutations, can emerge at varying timepoints in development and potentially become more pronounced with time. Thus, by phenotyping our mice at an adult age, we aim to target potentially more stable and more pronounced phenotypes. Both heterozygous (+/-) and homozygous (-/-) mutant mice were assessed where possible. Our control group comprised of 2 wild-type (+/+) littermates from each model (with the exception of *Shank3* where we had 3), pooled across all models. The models for *Arid1b*, *Chd8*, *Vps13b*, and *Sgsh*, were produced at The Centre for Phenogenomics and provided by the Canadian Mutant Mouse Repository (CMMR, Toronto ON). They were all created on a C57BL/6NCrl background (Charles River Laboratories, strain code 027). The mouse models *Fmr1* (Jackson Laboratory #003025) (43), 16p11.2 deletion (Jackson Laboratory #013128) (44) and *Shank3 (Δexon 4-9)* (Jackson Laboratory #017890) (45) were obtained from Jackson Laboratory and were backcrossed at least seven generations to C57BL/6NCrl (Charles River Laboratories, strain code 027). All procedures involving animals were performed in compliance with the Animals for Research Act of Ontario and the Guidelines

of the Canadian Council on Animal Care. The Centre for Phenogenomics (TCP) Animal Care Committee reviewed and approved all procedures conducted on animals at TCP.

The number of mice comprising each group is also listed in Table 1 and was determined following a power analysis with significance level α=0.05 and power β= 0.85.

Mouse Model – Common Name	Mouseline	Genotype	Number of Mice
Sgsh-Het	C57BL/6NCrl-*Sgsh*$^{em3(IMPC)Tcp}$/Cmmr	(+/-)	20
Sgsh-Hom	C57BL/6NCrl-*Sgsh*$^{em3(IMPC)Tcp}$/Cmmr	(-/-)	20
Fmr1	B6:129P2-*Fmr1*/n	(-/Y)	20
Arid1b	C57BL/6NCrl-*Arid1b*$^{em1(IMPC)Tcp}$/Cmmr	(+/-)	20
Shank3-Het (Δexon 4-9)	B6(Cg)-*Shank3*$^{tm1.2Bux}$/n	(+/-)	20
Shank3-Hom (Δexon 4-9)	B6(Cg)-*Shank3*$^{tm1.2Bux}$/n	(-/-)	20
16p11.2 deletion	B6.129S-Del(7Slx1b-Sept1)4Aam/n	(df/+)	20
Chd8	C57BL/6J-*Chd8*^{em1Tcp}	(+/-)	20
Vps13b	C57BL/6NCrl-*Vps13b*$^{em1(IMPC)Tcp}$/Cmmr	(+/-)	20
Wild-Type (WT)	-	(+/+)	21

Table 1: Mouse models used in the study given by their common name and official mouseline name. Genotype and number of mice used per model also listed.

Animal Preparation:

Mice were prepared as described by Zhou et al. (46). They were anesthetized using isoflurane (induced at 5% in medical oxygen, and then maintained at 1.5% through a face mask). Mice were positioned supine with four paws taped to electrodes on a pre-warmed platform for ECG recording and heart rate monitoring. Mouse body temperature was monitored by rectal thermometer (Indus Instruments, Houston, TX) and maintained around 36-37°C by a heated platform. Mouse hair on the whole chest was cleanly removed using hair-removal cream (Nair, Carter-Horner, Mississauga, Ontario). Finally, a prewarmed ultrasound gel (Aquasonic 100; Parker Laboratories, Orang, NJ) was used as a coupling medium between the transducer and mouse body for image acquisition.

Imaging:

A high frequency ultrasound imaging system (Vevo 2100, FUJIFILM VisualSonics Inc., Toronto) with a 30MHz linear array transducer was used for assessing cardiac structure, function and hemodynamics, mainly following an imaging protocol published previously (46,47). Unbiased screening of all models was performed using a standardised battery of measures utilizing four conventional function modalities of ultrasound imaging for a full cardiac assessment. Table 2 lists the imaging modalities, approaches/sections and measurements of interest. With the exception of HR, values for all metrics were obtained by averaging the measurements from three cardiac cycles in the same ultrasound recording.

All measures were obtained at least twice in different views/axes/traces (for example, from the left and right parasternal imaging windows or the short and long axis views of the heart). These measures were treated as duplicates/repeats in the data analysis.

Table 3 lists the cardiac parameters derived from the preliminary ultrasound measurements, and the formula for the related calculations.

Ultrasound imaging modalities	Technical description	Information and Measurements Obtained
B-Mode	• Two-dimensional grey-scale anatomical image • Spatial resolution: 100 μm (lateral), 50 μm (axial) • Max field-of-view (FOV): 14 mm • Max frame rate when image width reduced to minimum: 1000 fps	• Overall morphology of the heart • Guidance for M-mode and Doppler recordings • Distance and area measurements: Diameter of aortic orifice (AoD) during systole - measured from both left and right parasternal imaging windows
M-mode	• Recording of dynamic changes in position and dimension of the heart or vessel of interest in a chosen direction over a cardiac cycle. • Derive dimensional and functional parameters.	• Left Ventricle (LV) chamber diameter at end-systole (LV ESD) and end-diastole (LV EDD) – measured in both long and short axis views. • Left Ventricle (LV) anterior and posterior wall thickness at end-systole (LV AWes, PWes) and end-diastole (LV AWed, PWed) – measured in both long and short axis view. • Heart Rate (HR).
Doppler Colour Flow Mapping	• Visualize blood flow and its direction in different colors. • Qualitative demonstration of velocity distribution across heart chamber, orifice or vascular lumen. • Proper settings for the pulse repetition frequency (PRF)/velocity scale, gain and threshold of wall filtering.	• Guidance for pulse wave Doppler velocity measurement at the sites of interest. • Visualize the abnormal flow patterns such high velocity flow jets.
Pulse Wave Doppler	• Recording of blood flow velocity spectrum at site of interest. • Adjustable sample volume size to target vessel size. • Angle correction required for accurate measurement. Angle between ultrasound beam and flow less than 60 degrees.	• Peak E and A velocity ratio of mitral inflow for left ventricular diastolic function. • Velocity Time Integral (VTI) of flow through the vascular lumen such as the ascending aorta or aortic orifice for calculating the flow rate. • Heart Rate (HR).

Table 2: Four ultrasound imaging modalities used for full cardiac assessment, their technical description and the measurements obtained with each.

Measure	Full Name	Class – Acquisition Method	Type	Acquisition Details
AoD	Diameter of aortic orifice during systole	Measured	Morphological	Measured in both left and right parasternal imaging windows.
VTI	Velocity Time Integral of flow through the ascending aorta.	Measured	Functional	
LVESD	Left Ventricle (LV) chamber diameter at end-systole	Measured	Morphological	Measured in both long and short axis views of the heart.
LVEDD	Left Ventricle (LV) chamber diameter at end-diastole	Measured	Morphological	Measured in both long and short axis views of the heart.
LV AWes	Left Ventricle (LV) anterior wall thickness at end-systole	Measured	Morphological	Measured in both long and short axis views of the heart.
LV AWed	Left Ventricle (LV) anterior wall thickness at end-diastole	Measured	Morphological	Measured in both long and short axis views of the heart.
LV PWes	Left Ventricle (LV) posterior wall thickness at end-systole	Measured	Morphological	Measured in both long and short axis views of the heart.
LV PWed	Left Ventricle (LV) posterior wall thickness at end-diastole	Measured	Morphological	Measured in both long and short axis views of the heart.
HR	Heart Rate	Measured	Functional	Measured from all M-mode, and Doppler recordings
EA ratio	Peak E and A velocity ratio of mitral inflow for left ventricular diastolic function	Measured	Functional	

LVSV	Left Ventricle (LV) stroke volume	Calculated	Functional	$LVSV = \pi \cdot VTI \cdot \left(\frac{AoD}{2}\right)^2$
CO	Cardiac output	Calculated	Functional	$CO = LVSV \cdot \mathrm{HR}$
LVFS	Left Ventricle (LV) fractional shortening	Calculated	Functional	$LVFS = 100 \cdot \frac{\mathrm{LVEDD} - LVESD}{LVEDD}$
LV AWT	Left Ventricle (LV) anterior wall thickening (%)	Calculated	Functional	$LVAWT = 100 \cdot \frac{\mathrm{LVAWes} - LVAWed}{LVAWed}$
LV PWT	Left Ventricle (LV) posterior wall thickening (%)	Calculated	Functional	$LVPWT = 100 \cdot \frac{\mathrm{LVPWes} - LVPWed}{LVPWed}$

Table 3: All the morphological and functional cardiac measures used in the study. The acronym, full name, and type (morphological or functional) of each measurement are given. For each measurement, the method of acquisition (termed "class") (measured or calculated) is given along with the acquisition details (how it was measured (with ultrasound imaging) or calculated).

Data analysis:

Statistical analysis was performed in `R3.6.1` (48) using the `RStudio` interface (49) and the `brms` (50,51), loo (52) and `bayesplot` packages (53–56).

For each measure, we fit a Bayesian model with partial pooling to the *Z*-score values of our data, with mouse group and intercept as predictors and a random effect of mouse ID to account for redundancy in certain measures (measured more than once in different axes). We evaluated the need to account for a heteroscedasticity by comparing a model where variance of the posterior distribution varies between mouse groups (equation 1-A) versus a model with uniform variance across all groups (equation 1-B). All equations, including the priors used, can be found in equation 1.

(A)

$$y_i \sim \mathcal{N}\left(\mu_{j_i k_i m_i},\, \sigma^2_{j_i k_i}\right) \qquad \textit{Heteroscedastic model}$$

$$\mu_{j_i k_i m_i} = \beta^0_{j_i k_i} + \beta^1_{j_i k_i} \cdot group_{j_i k_i} + \beta_{m_i}$$

$$\sigma_{jkm} = \gamma^0_{jk} + \gamma^1_{jk} \cdot group_{jk}$$

$$\beta^0_{j_i k_i} \sim Student^{+}(0,\, 2.5, 3) \qquad \textit{Intercept prior}$$

$$\beta^1_{j_i k_i} \sim Unif(-\infty\,,\, +\infty) \qquad \textit{Group effect prior}$$

$$\beta_{m_i} \sim \mathcal{N}\left(0,\, \sigma^2_{m_i}\right) \qquad \textit{Random effect prior}$$

$$\sigma_{m_i} \sim Student^{+}(0,\, 2.5, 3) \qquad \textit{Random effect standard deviation prior}$$

$$\gamma^0_{jk} \sim Student^{+}(0,\, 2.5, 3) \qquad \textit{Intercept prior of standard deviation } \sigma_{jkm}$$

$$\gamma^1_{jk} \sim Unif(-\infty\,,\, +\infty) \qquad \textit{Group effect prior of standard deviation } \sigma_{jkm}$$

(B)

$$y_i \sim \mathcal{N}\left(\mu_{j_i k_i m_i},\, \sigma^2_{jk}\right) \qquad \textit{Homoscedastic model}$$

$$\mu_{j_i k_i m_i} = \beta_0 + \beta_1 \cdot group_{j_i k_i} + \beta_{m_i}$$

$$\beta^0_{j_i k_i} \sim Student^{+}(0,\, 2.5, 3) \qquad \textit{Intercept prior}$$

$$\beta^1_{j_i k_i} \sim Unif(-\infty\,,\, +\infty) \qquad \textit{Group effect prior}$$

$$\beta_{m_i} \sim \mathcal{N}\left(0,\, \sigma^2_{m_i}\right) \qquad \textit{Random effect prior}$$

$$\sigma_{m_i} \sim Student^{+}(0,\, 2.5, 3) \qquad \textit{Random effect } \beta_{m_i} \textit{ standard deviation prior}$$

Equation 1: (A) Heteroscedastic Bayesian model. (B) Homoscedastic Bayesian model. The Z-scored data for each observation (i) of every cardiac measure (j), mouse group (k) and mouse ID (m), y_i, is modeled as a normal distribution with a mean ($\mu_{j_i k_i m_i}$) and a variance which either varies with measure and mouse group (σ^2_{jkm}) (heteroscedastic) or varies only with measure (σ^2_{jk})

(homoscedastic). $\beta^0_{j_i k_i}$ *is the intercept and* $\beta^1_{j_i k_i}$ *is the group effect of the mean* ($\mu_{j_i k_i m_i}$). β_{m_i} *is the random effect of mouse ID to account for repeated measurements and* σ_{m_i} *is the standard deviation of the normal prior on* β_{m_i}. γ^0_{jk} *is the intercept and* γ^1_{jk} *is the group effect of the standard deviation* σ_{jkm} *of* y_i. $Student^+(0, 2.5, 3)$ *is the half-student-t distribution with zero mean, scaling factor 2.5 and 3 degrees of freedom.*

The comparison of the two models was performed using the pareto-smoothed-importance-sampling leave-one-out cross-validation (*PSIS LOO CS*) method (57) in the loo package (52). For each measure, we then used the model that performed the best (Table 4).

For all sets of measures, we used the posterior distribution to obtain estimates for the mean for each genetic group. However, for measures fit using the heteroscedastic model, we obtained variance (sigma) for each genetic group, while measures fit using the homoscedastic model, we obtained a single posterior distribution for the variance (sigma) shared amongst genetic groups.

Once the posterior distributions were obtained a series of comparisons were performed. Specifically, each mutant group (total of 9) was compared to the WT control group for each cardiac measure (total of 15), for a total of 135 comparisons. Additionally, each mutant group (total of 9) was compared to every other mutant group per cardiac measure (total of 15), for a total of 540 comparisons.

For each posterior distribution we obtained the following metrics: median, mean, 89% credible intervals (CIs) and probability of direction (*pd*) (58,59). We controlled for the false discovery rate based on methods presented by J. Storey (60). Firstly, we calculated the posterior error probability (*PEP*) using: $PEP = 1 - pd$. PEP was used as a Bayesian p-value equivalent. Subsequently, we performed a correction on the PEP values using the formula:

$$PEP_{i\_adjusted} = \frac{p_{prior} \cdot PEP_{i\_cumulative}}{p_{prior} \cdot PEP_{i\_cumulative} + (1 - p_{prior}) \cdot (1 - PEP_{i\_cumulative})}$$

Equation 2: Calculation of adjusted PEP of rank i to correct for multiple comparisons. p_{prior} is the prior estimate of the PEP value (p-value). Each $PEP_{i\_cumulative}$ is obtained after ranking the PEP values in increasing order (rank given by i) and adding all PEP values of less or equal rank to get $PEP_{I\_cumulative}$.

The prior estimate of the *PEP* value (p_{prior}) was obtained from the histogram of the *PEP* values (chosen bin size 0.05), using the following equation:

$$p_{prior} = \frac{N_{\{-1\}}}{N}$$

Equation 3: Estimate of prior PEP value. $N_{\{-1\}}$ is the sum of counts in all bins except for the first bin of the PEP histogram. N is the sum of counts in all bins. Chosen bin size was 0.05.

$PEP_{adjusted} \leq 0.05$ was considered to be of high confidence or significant.

Principal Component Analysis and Total Correlation

Principal Component Analysis (PCA) and total correlation were used to explore the redundancy in our cardiac measures and genetic groups. This corresponds to comparing the genetic group by cardiac measure matrix of posterior means against its transpose. Firstly, for visual inspection, for each data matrix orientation (original and transposed), bootstrapping with replacement was performed to determine the median eigenvalue density for each PC component (as captured by the scree plot) along with the associated 95% confidence intervals. Secondly, to quantify the redundancy, total correlation was calculated (61).

Total correlation is sensitive to dimension (61). Thus, to make the total correlation comparable across both datasets, each dataset was iteratively downsampled to the lowest

dimension ($N_{genetic\ groups} \times N_{\text{genetic groups}}$) by performing random selection without replacement of columns or rows where appropriate. For each dataset, the mean and standard deviation of the total correlation across all iterations were calculated. Further details on the total correlation calculation can be found in the Supplementary Materials.

Results

The type of model (heteroscedastic or homoscedastic) run per cardiac measure is shown in Table 4. Depending on the model, coefficient estimates (posterior distributions) were obtained either only for the median or for both the median and variance of the coefficients. The coefficient estimates for the median are shown in Figure 1.

Cardiac Measure	Type of Bayesian Model
Aorta Diameter (AoD)	Heteroscedastic
Velocity Time Integral (VTI)	Homoscedastic
Peak E to A Velocity Ratio	Homoscedastic
Left Ventricular (LV) chamber diameter (end-systole)	Heteroscedastic
Left Ventricular (LV) chamber diameter (end-diastole)	Homoscedastic
Left Ventricular (LV) anterior wall thickness (end-systole)	Heteroscedastic
Left Ventricular (LV) anterior wall thickness (end-diastole)	Homoscedastic
Left Ventricular (LV) posterior wall thickness (end-systole)	Heteroscedastic
Left Ventricular (LV) posterior wall thickness (end-diastole)	Heteroscedastic
Left Ventricular (LV) anterior wall thickening	Homoscedastic
Left Ventricular (LV) posterior wall thickening	Heteroscedastic
Heart Rate (HR)	Heteroscedastic
Cardiac Output (CO)	Heteroscedastic
Left Ventricular Fractional Shortening (LVFS)	Homoscedastic
Left Ventricular Stroke Volume (LVSV)	Heteroscedastic

Table 4: Type of Bayesian model used for each cardiac measure. One Bayesian model was run per cardiac measure comparing all genetic groups. For each model, the variance was either considered constant across genetic groups (homoscedastic) or varying between genetic groups (heteroscedastic).

We determined the number of "high confidence" or "significant" ($PEP_{adjusted} \leq 0.05$) tests per genetic group, compared to all tests performed for that group. The fraction of high-confidence tests was used as a metric of difference compared to the reference group. The higher

the fraction, the more (measures with) significant differences between the groups. Similarly, for each cardiac measure the number of high-confidence tests was calculated (relative to the total number of tests). In this case, it was interpreted as the prevalence of each cardiac measure in an abnormal cardiac phenotype. The higher the fraction, the more often would that cardiac measure be abnormal (relative to the reference group).

Comparing ASD-related genetic models to littermate wild-type (WT) controls

From our results, the differences between mutant groups and WT controls varied between mutant groups in both number and magnitude. The mutant group with the greatest number of significant differences in cardiac phenotype relative to WT controls was the 16p11.2 (deletion) group (6/15 measures) with the *Arid1b* $^{(+/-)}$ and *Fmr1*$^{(-/-)}$ groups following (3/15 measures). Next were the *Shank3*$^{(+/-)}$ *(Δexon 4-9), Chd8*$^{(+/-)}$ and *Sgsh*$^{(-/-)}$ groups (2/15 measures each but not in all the same cardiac measures) (Figure 3A). In all comparisons to WT controls, the cardiac measures that were most often found abnormal were, the left ventricular (LV) anterior wall thickening (LVAWT) (3/9 groups), LV chamber diameter at end-diastole (LVEDD) (3/9 groups), and LV anterior wall thickness at end-diastole (LVAWed) (3/9 groups) and end-systole (LVAWes) (2/9 groups) (Figure 3B). Overall, there were mainly morphological differences, but functional differences were also present.

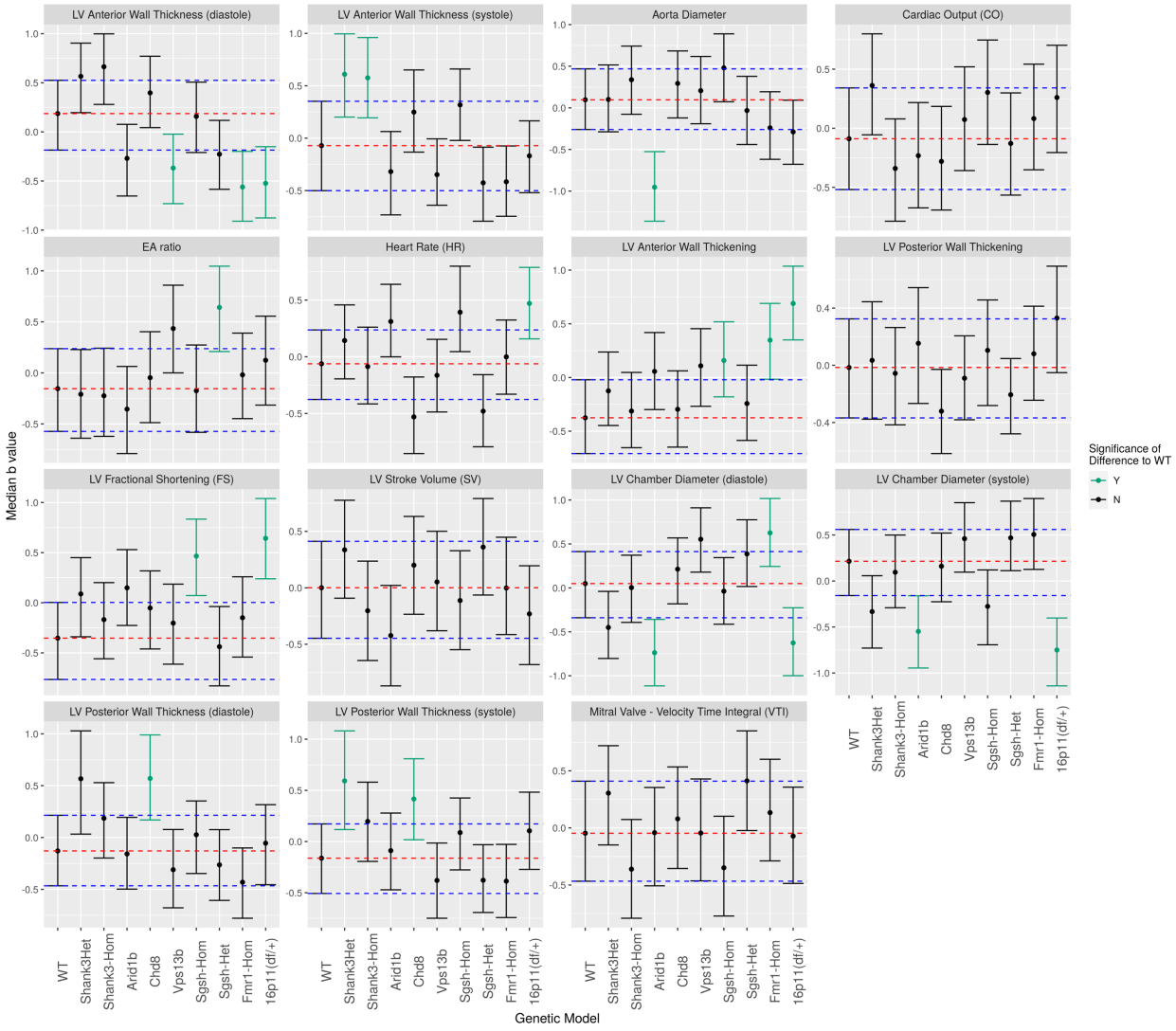

Figure 1: Median coefficient estimates (b-values) per genetic group per cardiac measure. Unadjusted 89% Credible Intervals (CIs) shown as whiskers. The blue dashed lines indicate the upper and lower 89% CIs for the WT control group. The red dashed line indicates the median of the WT control group. Green colour indicates the groups that are significantly different from WT controls. Significance assigned based on FDR corrected q values.

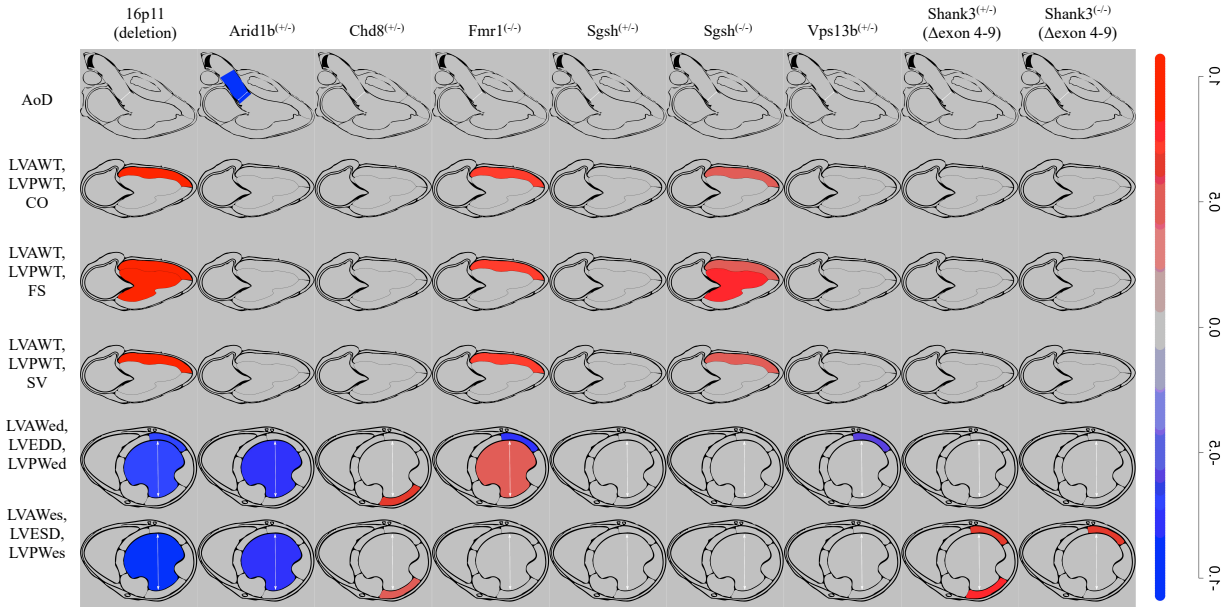

Figure 2: Normalised median differences per cardiac measure between each mutant mouse group and wild-type controls (WTs). The colour gradient was generated mapping to the range of normalised median values; only the data from the high-confidence (significant) tests across all cardiac measures and groups were used. For all other (non-significant) tests, a grey colour was assigned, same as the background. Each column corresponds to a mutant mouse group and each row depicts one or a set of cardiac measures. Abbreviations: AoD – Aorta Diameter; LVAWT – left ventricular anterior wall thickening; LVPWT – left ventricular posterior wall thickening; CO – cardiac output; FS – fractional shortening; LVAWed – left ventricular end-diastolic anterior wall thickness; LVEDD – left ventricular end-diastolic (chamber) diameter; LVPW – left ventricular end-diastolic posterior wall thickness; LVAWes – left ventricular end-systolic anterior wall thickness; LVESD – left ventricular end-systolic (chamber) diameter; LVPWes – left ventricular end-systolic posterior wall thickness.

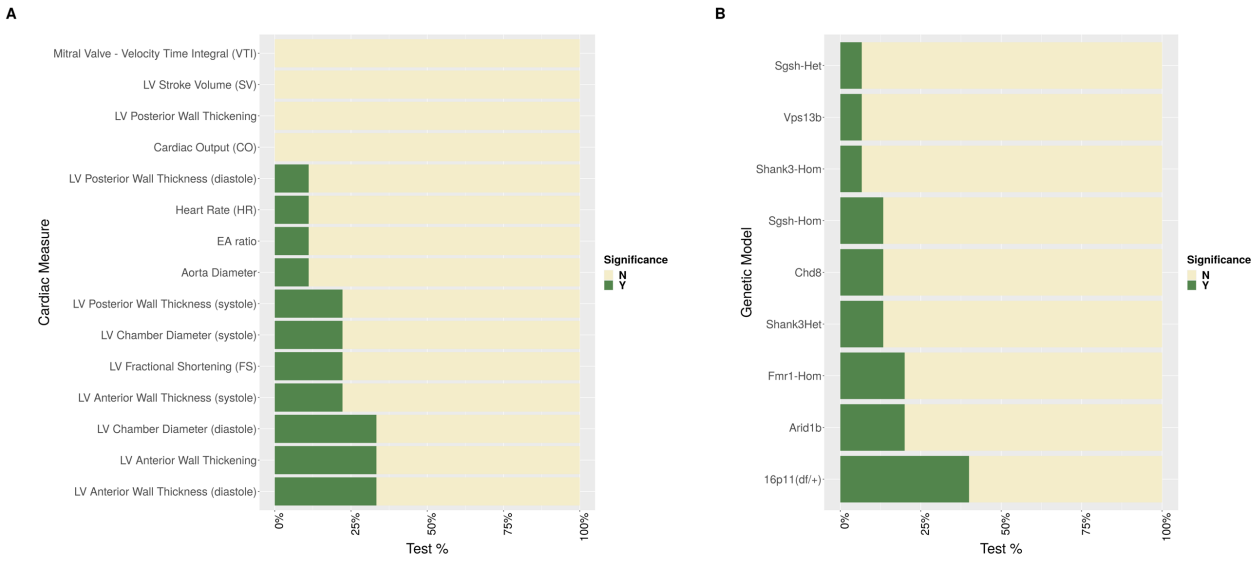

Figure 3: Barplots indicating the percent of significant (high confidence) comparisons (tests) between mutants and WT controls. (A) For each cardiac measure all ASD-related mutant groups were compared to WT controls; the same total number of comparisons (tests) was conducted for all cardiac measures. The green bar indicates the percent of significant comparisons (tests) for each cardiac measure. (B) Similar to (A), each ASD-related mutant group was compared to WT controls for all cardiac measures; same number of comparisons (tests) was conducted for all mutant groups. The green bar indicates the percent of significant comparisons (tests) for each group.

Comparing ASD-related genetic mouse groups

To explore the heterogeneity amongst mutant groups, we identified the cardiac measures that differed most between groups (Figure 4A), the mutant groups with most differences from all other groups (Figure 4B), and the mutant group pairs with the most differences.

A greater number of significant differences was present between mutant groups than when mutant groups were compared to WT controls. The measures driving the inter-group variation tended to be associated more with morphological changes than functional changes (Figure 4A). Specifically, the mutant groups firstly differ in LV chamber diameter at end-diastole (LVEDD) (significance found in 18/138 pairwise comparisons) and, secondly, in LV anterior wall thickness at end-systole and end-diastole (LVAWes, LVAWed) (17/138 pairwise comparisons each). Thirdly they differ in LV chamber diameter at end-systole (LVESD) (16/138

pairwise comparisons), followed by heart rate (HR) (13/138 pairwise comparisons). The 16p11.2 (deletion) and *Sgsh*$^{(+/-)}$ groups had the most differences from all other mutant groups (38/1080 pairwise comparisons), followed by the *Arid1b*$^{(+/-)}$ (36/120 pairwise comparisons) and *Chd8*$^{(+/-)}$ (33/120 pairwise comparisons) groups (Figure 4B).

Conducting pairwise mutant group analysis, the *Shank3*$^{(+/-)}$ *(Δexon 4-9)* - *Sgsh*$^{(+/-)}$ and the *Chd8*$^{(+/-)}$ - 16p11.2 (deletion) pairs had the greatest number of significant differences in cardiac measures (8/15 measures), followed by the *Shank3*$^{(-/-)}$ *(Δexon 4-9)* - 16p11.2 (deletion) and *Arid1b*$^{(+/-)}$ - *Sgsh*$^{(+/-)}$ pairs (7/15 measures each).

Of interest is the comparison of the distributions in Figures 3A and 4A. When compared to each other, mutant groups tended to differ more in morphological measures than in functional measures (Figure 4A), but when compared to WT controls, they tended to differ roughly equally in both (Figure 3A).

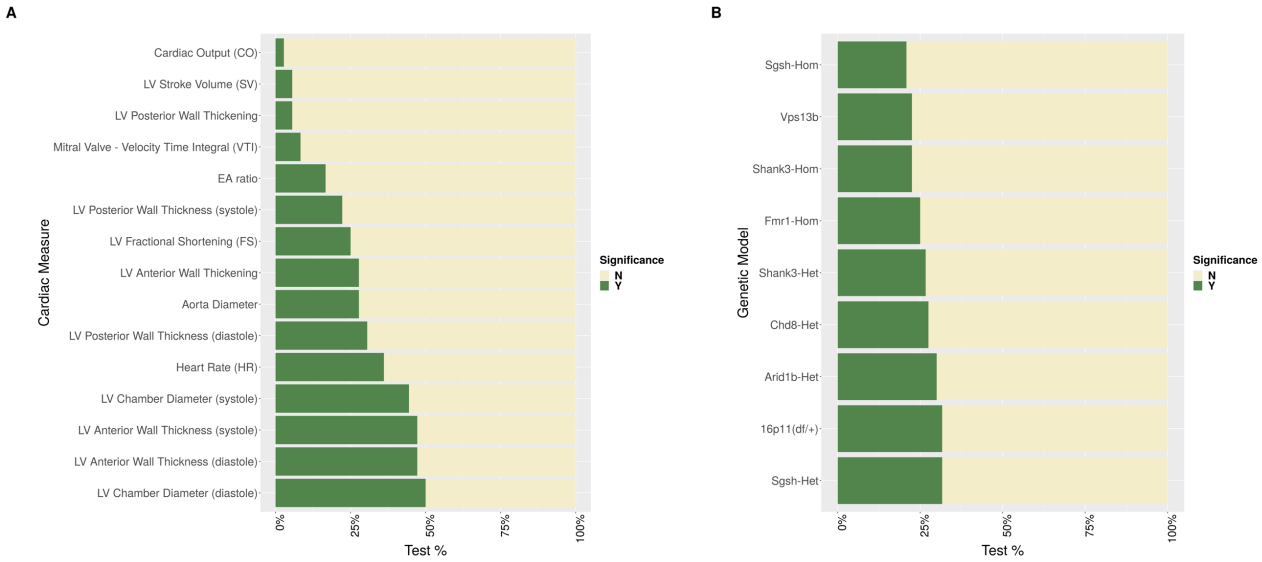

Figure 4: Barplots indicating the percent of significant (high confidence) comparisons (tests) between all ASD-related genetic mutant groups. (A) For each cardiac measure all ASD-related mutant groups were compared to each other; the same total number of comparisons (tests) was conducted for all cardiac measures. The green bar indicates the percent of significant comparisons (tests) for each cardiac measure. (B) Similar to (A), each ASD-related mutant group was compared to every other mutant group, for all cardiac measures; same number of comparisons (tests) was conducted for all mutant groups. The green bar indicates the percent of significant comparisons (tests) for each group.

Principal Component Analysis and Total Correlation

For the 15 cardiac measures, PCA revealed that 9 principal components were required to account for ~99% of the variance in the data. This can be explained by the fact that, from the set of 15 measures, 5 were not directly measured but were calculated using others, as described in Methods. For the 10 genetic groups, PCA also revealed that 9 principal components were required to account for ~99% of the variance in the data. Therefore, there doesn't seem to be any pattern of similarity (redundancy) between the mutant groups with regard to cardiac phenotype.

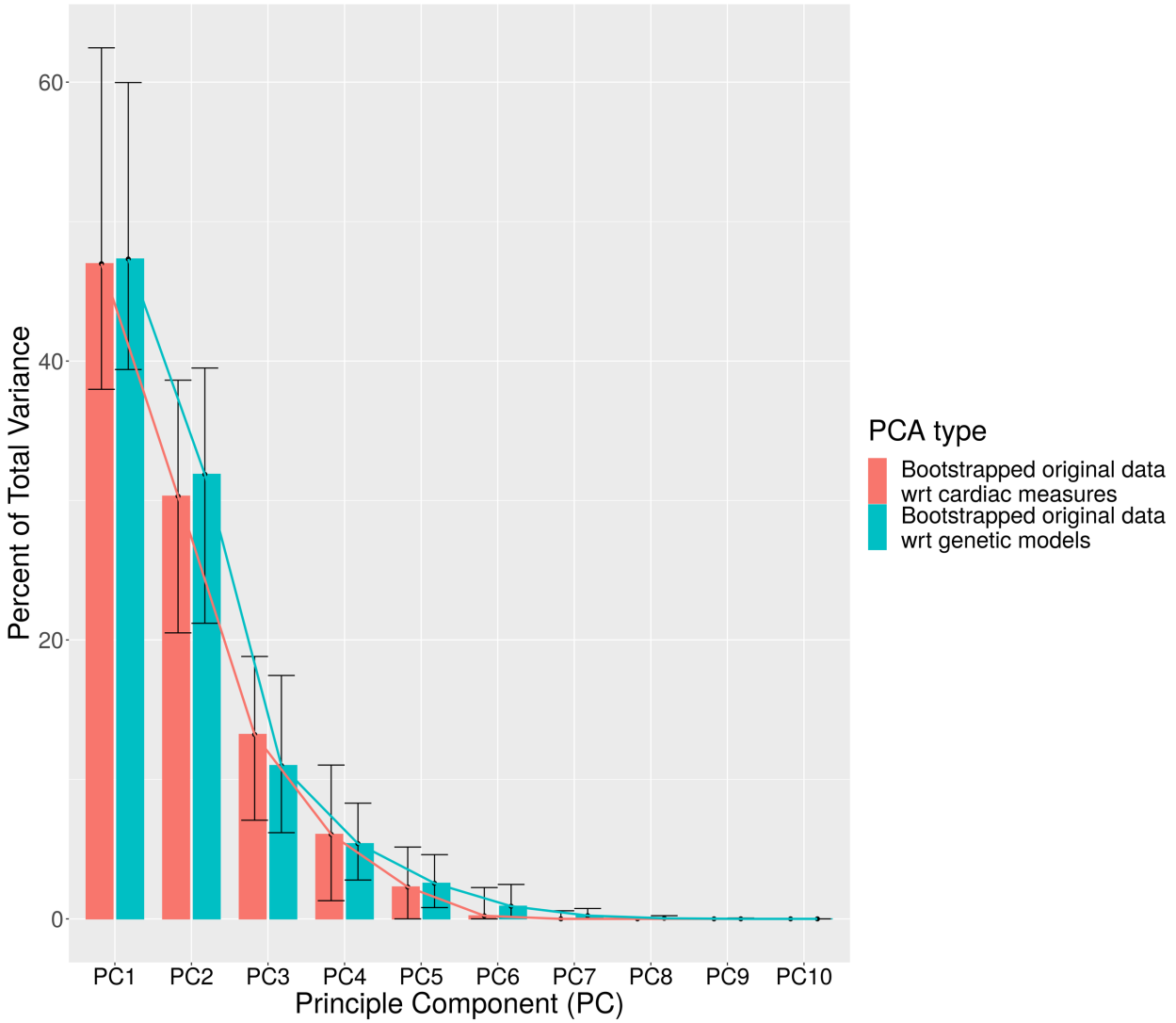

Figure 2: Scree plot of PCA on cardiac measures and PCA on genetic models. Bootstrapping with replacement of the data was performed to determine the median eigenvalue density for each PC component along with the associated 95% confidence intervals. The bootstrapped data are shown along with the bootstrapped median values and 95% confidence intervals. The estimated decay curve is also mapped.

To inspect the comparable redundancy between cardiac measures and genetic groups, the total correlation was computed (Table 4). The total correlation of 15 cardiac measures was 66.18 and of 10 genetic groups was 10.79. As total correlation is sensitive to the number of dimensions, we randomly downsampled both datasets to 10 dimensions with 1000 permutations (reporting mean +/- standard deviation). The total correlation of the downsampled cardiac

measures was 18.15 +/- 1.3 and of the downsampled genetic groups was 19.36 +/- 1.26. Thus, the total correlation, and therefore redundancy, is comparable between cardiac measures and genetic groups. Amongst cardiac measures and amongst genetic groups, respectively, some redundancy or correlation exists since for random data the total correlation would be zero.

	Total Correlation Original Dimensions	Total Correlation Downsampled Data	Total Correlation Downsampled Data Standard Deviation
Original-Cardiac Measures	66.18	18.15	1.3
Original-Genetic Groups	10.79	19.36	1.26

Table 4: Total correlation values per dataset. First column is the total correlation of the original datasets. In the second and third column are the mean total correlation and standard deviation respectively, across all iterations, for the downsampled data.

Discussion

Our analysis revealed small-scale alterations in cardiac structure and function in ASD compared to WT, mirroring the clinical reports. However, significant differences of note were present. Firstly, the alterations each mutant group presented to WT controls were largely not consistent between groups. Therefore, the heterogeneity characterising ASD in other phenotypes (7,8) is recapitulated here. Specifically, when compared to each other, mutant groups presented a greater number of significant differences than when compared to WT controls. As mentioned, this is possible due to certain mutant groups differing insignificantly from WT controls in an opposite fashion (for the same cardiac measure). Secondly, mutant groups tended to differ primarily in measures of LV structure, while when compared to WT controls, they tended differ in both morphological and functional measures, with a small prevalence of the former. However, there was overlap in the overall associated measures with HR and LV chamber diameter and anterior wall thickness being strong contributors in both cases. Moving forward, it would be of

interest to expand this work to include more ASD-related genetic models and further assess the emerging patterns.

As previously mentioned, the available clinical literature on the cardiac phenotype of ASD patients is not extensive and not always consistent. Nevertheless, with our standardised protocol we interrogated the cardiac phenotype of our genetic models and compared our findings to the clinically documented abnormalities associated with the corresponding ASD genetic mutations. This information can be found in the Supplementary Materials. Overall, our screening process captures the abnormalities reported clinically for each genetic mutation. For example, in the *Arid1b* $^{(+/-)}$ group, in agreement with the clinical observations, we observed arterial stenosis at the level of the aortic valve. We also see evidence of the common cardiac abnormalities associated with ASD, for example autonomic dysregulation (manifested as abnormal HR). A detailed per-model account of this comparison can be found in the Supplementary Materials.

Given the heterogeneity observed, it is valuable to determine how it compares to a standardised categorisation of our genetic groups. One such categorisation can be found in the SFARI Gene database (Simons Foundation; http://gene.sfari.org/) (62) which has assigned a score to each genetic variant quantifying how closely each genetic group is linked to ASD. According to the SFARI Gene database, the 16p11.2 (deletion), *Arid1b*$^{(+/-)}$, *Fmr1*$^{(-/-)}$, *Shank3 (Δexon 4-9)*, *Chd8*$^{(+/-)}$, *Vps13b*$^{(+/-)}$ groups hold a high score and the *Sgsh* group holds a lower score. However, even when assessing our results with the SFARI score in mind, a pattern cannot be identified. As shown in Figure 3B, considering the number of differences to WT controls, certain groups with a high SFARI score rank high (16p11.2 (deletion), *Arid1b*$^{(+/-)}$, *Fmr1*$^{(-/-)}$, *Shank3 (Δexon 4-9)*), while others rank low (*Chd8*$^{(+/-)}$, *Vps13b*$^{(+/-)}$). The *Sgsh* group with a low SFARI score ranks somewhere between the two. This discrepancy between SFARI gene score

and severity of cardiac phenotype in each group could be driven by different expression levels of the associated gene between the brain and the heart.

Consequently, it seems unfeasible, with this type of assessment, to identify an overarching ASD-related cardiac phenotype, shared between all individual genetic mutant groups and setting them apart from WT controls. It seems more likely that there would be subgroups of ASD-related models, potentially not based on how closely they are linked to ASD (SFARI Gene score), each with a different cardiac phenotype compared to WT controls. This is something to be explored further in the future.

Knowing the abnormalities present, allows us to choose alternate measures to explore more closely the observed changes and probe the underlying mechanisms. Additionally, categorising measures as morphological or functional can offer insight about common etiology of the models' cardiac phenotype. For example, the Sinoatrial Node (SAN) is the principal pacemaker of the heart, it is characterised by cellular heterogeneity and its formation and function are controlled by a series of upstream factors (63,64). Its cells have been clustered based on their downstream function, revealing a wide range of targets (64). We could then hypothesise that a disruption affecting the formation of SAN (starting at embryonic day 9.5) could result in a spectrum of functional abnormalities across various genetic groups (depending on the origin and type of the disruption). Similarly for structural abnormalities.

The cardiac phenotype of each of our ASD mouse mutant groups was consistent with results seen in the corresponding human population to the extent that a direct comparison is possible (see supplementary materials). For example, in the *Arid1b* $^{(+/-)}$ group, in agreement with the corresponding clinical reports (5), we observed arterial stenosis at the level of the aortic valve. Similarly, the cardiac abnormalities associated with ASD as a whole (as reported in

literature) are also observed across all our ASD groups. For example, autonomic regulation is impaired in the autism population which is consistent with our observations that HR was one of the main differing measures between ASD mutant groups and WT controls.

Finally, Principal Component Analysis (PCA) and total correlation comparison revealed a comparable redundancy between the cardiac measures and the genetic groups, while ensuring the outcome wasn't solely driven by underlying noise. One would expect cardiac measures to have a larger redundancy (since all measures are related to the heart), compared to the genetic groups (each was created to carry a different genetic modification). However, this result indicates that the cardiac measures used in this study are more independent than one would expect (with some correlation amongst them still present). Thus, once again, confirming that our UBM protocol captures various dimensions of cardiac functionality, as intended, and can be used as an effective screening protocol. For the genetic groups, this result indicates there is some correlation between the ASD-related models but overall, as mentioned previously, the heterogeneity characteristic of ASD is recapitulated in the cardiac phenotype as well.

Limitations

There are certain limitations to this work which must be considered. Firstly, this work was conducted using adult mice. However, various genetically driven cardiac abnormalities, and especially CHD, occur early in life. So, by screening in adult age, there is a risk of observing a modified state which resulted from various adaptive mechanisms acting throughout development. Secondly, only male mice were used in the study. Given the known sex differences in ASD (63) and cardiac function (64), we recognise it may be of value to repeat this work on female mice. Thirdly, the downsampling procedure used for the calculation of total correlation is

not a standard approach for comparing two datasets of differing dimensions. So further investigation is needed to verify this approach. Finally, a direct comparison between our results and the clinical literature is not possible because clinical studies often employ different study designs (assessment protocols, sample sizes etc) and recruit both male and female patients. Namely, in this study we did not perform direct assessment of the atrioventricular septum, the right side of the heart, the extracardiac space or the conduction system of the heart, which are widely mentioned in many of the clinical reports, as is shown in Table 1 of the Supplementary Materials. However, potential links can be inferred based on knowledge of the overall structure and function of the cardiovascular system. As the number of ASD-related genetic models screened with this protocol increases and as the corresponding clinical data amounts, we will be able to make even more concrete comparisons.

Conclusion

This work sheds light on the spectrum of cardiac abnormalities associated with ASD-related genetic abnormalities. The heterogeneity characterising ASD in other phenotypes is recapitulated here, with more differences seen between mutant groups than when compared to WTs. Alterations were small in scale, but significant, and further exploration of more models is needed to validate the observed patterns. Our high frequency ultrasound imaging protocol as a method of cardiac assessment provides a well-rounded view of cardiac structure and function, effectively capturing the clinically reported cardiac abnormalities. Thus, it can be used as a screening protocol moving forward. The detected cardiac abnormalities can then be further examined using potentially more sensitive methods to explore their underlying mechanisms. By classifying cardiac measures as morphological or functional, the etiology of mutant phenotype

can be better understood, and any common underlying mechanisms can be elucidated. Clinically, knowledge of the cardiac abnormalities associated with ASD can be greatly beneficial as, even non-lethal cardiac abnormalities can impact the normal development and function of various other biological systems, such as the brain. In addition, the presence of specific cardiac abnormalities may provide mechanistic insights for a patient's ASD subtype.

Abbreviations

ASD: Autism Spectrum Disorder

CHD: Congenital Heart Disease

UBM: Ultrasound Bio-Microscopy

LV: Left Ventricle

WT: Wild-Type

HET: Heterozygous (+/-)

HOM: Homozygous (-/-)

AoD: Aorta Diameter

HR: Heart Rate

LVAWed: Left Ventricular Anterior Wall Thickness at End-Diastole

LVAWes: Left Ventricular Anterior Wall Thickness at End-Systole

LVEDD: Left Ventricular Chamber Diameter at End-Diastole

LVESD: Left Ventricular Chamber Diameter at End-Systole

LVPWed: Left Ventricular Posterior Wall Thickness at End-Diastole

LVPWes: Left Ventricular Posterior Wall Thickness at End-Systole

LVAWT: Left Ventricular Anterior Wall Thickening

LVPWT: Left Ventricular Posterior Wall Thickening

FS: Fractional Shortening

CO: Cardiac Output

LVSV: Left Ventricular Stroke Volume

sys: systole

di: diastole

PCA: Principal Component Analysis

MRI: Magnetic Resonance Imaging

ECG: Electrocardiography

References

1. Limperopoulos C, Tworetzky W, McElhinney DB, Newburger JW, Brown DW, Robertson RL, et al. Brain volume and metabolism in fetuses with congenital heart disease: Evaluation with quantitative magnetic resonance imaging and spectroscopy. Circulation. 2010;121(1):26–33.
2. Kaltman JR, Di H, Tian Z, Rychik J. Impact of congenital heart disease on cerebrovascular blood flow dynamics in the fetus. Ultrasound in Obstetrics and Gynecology. 2005;25(1):32–6.
3. Sun L, Macgowan CK, Sled JG, Yoo SJ, Manlhiot C, Porayette P, et al. Reduced fetal cerebral oxygen consumption is associated with smaller brain size in fetuses with congenital heart disease. Circulation. 2015;131(15):1313–23.
4. Homsy J et al. De novo mutations in Congenital Heart Disease with Neurodevelopmental and Other Birth Defects. Science. 2015.
5. Pierpont ME, Brueckner M, Chung WK, Garg V, Lacro R v., McGuire AL, et al. Genetic Basis for Congenital Heart Disease: Revisited: A Scientific Statement from the American Heart Association. Vol. 138, Circulation. 2018. 653–711.
6. Tsao PC, Lee YS, Jeng MJ, Hsu JW, Huang KL, Tsai SJ, et al. Additive effect of congenital heart disease and early developmental disorders on attention-deficit/hyperactivity disorder and autism spectrum disorder: a nationwide population-based longitudinal study. European Child and Adolescent Psychiatry. 2017;26(11):1351–9.
7. Amaral DG. The promise and the pitfalls of autism research: An introductory note for new autism researchers. Brain Research. 2011;1380(916):3–9.
8. Amaral D, Dawson G, Geschwind D. Autism Spectrum Disorders [Internet]. Oxford University Press, USA; 2011. (EBSCO ebook academic collection). Available from: https://books.google.ca/books?id=Prf0InCqQS0C
9. Tyler C v., Schramm SC, Karafa M, Tang AS, Jain AK. Chronic Disease Risks in Young Adults With Autism Spectrum Disorder: Forewarned Is Forearmed. AJIDD. 2011.
10. Hoffman JIE, Kaplan S. The incidence of congenital heart disease. Journal of the American College of Cardiology [Internet]. 2002;39(12):1890–900. Available from: http://dx.doi.org/10.1016/S0735-1097(02)01886-7
11. Wu W, He J, Shao X. Incidence and mortality trend of congenital heart disease at the global, regional, and national level, 1990-2017. Medicine (United States). 2020;99(23).
12. Sadowski SL. Congenital Cardiac Disease in the Newborn Infant: Past, Present, and Future. Critical Care Nursing Clinics of North America. 2009;21(1):37–48.
13. Marino BS, Lipkin PH, Newburger JW, Peacock G, Gerdes M, Gaynor JW, et al. Neurodevelopmental outcomes in children with congenital heart disease: Evaluation and management a scientific statement from the american heart association. Circulation. 2012;126(9):1143–72.
14. Sigmon ER, Kelleman M, Susi A, Nylund CM, Oster ME. Congenital heart disease and autism: A case-control study. Pediatrics. 2019;144(5).
15. Miller SP, McQuillen PS, Hamrick S, Xu D, Glidden D v., Charlton N, et al. Abnormal brain development in newborns with congenital heart disease. New England Journal of Medicine. 2007;357(19):1928–38.
16. Licht DJ, Shera DM, Clancy RR, Wernovsky G, Montenegro LM, Nicolson SC, et al. Brain maturation is delayed in infants with complex congenital heart defects. J Thorac Cardiovasc Surg. 2009;137(3):529–37.
17. Clouchoux C, Kudelski D, Gholipour A, Warfield SK, Viseur S, Bouyssi-Kobar M, et al. Quantitative in vivo MRI measurement of cortical development in the fetus. Brain Structure and Function. 2012;217(1):127–39.

18. Ortinau CM, Mangin-Heimos K, Moen J, Alexopoulos D, Inder TE, Gholipour A, et al. Prenatal to postnatal trajectory of brain growth in complex congenital heart disease. NeuroImage: Clinical [Internet]. 2018;20(August):913–22. Available from: https://doi.org/10.1016/j.nicl.2018.09.029
19. Gaynor JW, Wernovsky G, Jarvik GP, Bernbaum J, Gerdes M, Zackai E, et al. Patient characteristics are important determinants of neurodevelopmental outcome at one year of age after neonatal and infant cardiac surgery. Journal of Thoracic and Cardiovascular Surgery. 2007;133(5):1344–53.
20. Croen LA, Zerbo O, Qian Y, Massolo ML, Rich S, Sidney S, et al. The health status of adults on the autism spectrum. Autism. 2015;19(7):814–23.
21. Miot S, Akbaraly T, Michelon C, Couderc S, Crepiat S, Loubersac J, et al. Comorbidity Burden in Adults With Autism Spectrum Disorders and Intellectual Disabilities—A Report From the EFAAR (Frailty Assessment in Ageing Adults With Autism Spectrum and Intellectual Disabilities) Study. Frontiers in Psychiatry. 2019;10(September).
22. Dawson S, Glasson EJ, Dixon G, Bower C. Birth defects in children with autism spectrum disorders: A population-based, nested casec-control study. American Journal of Epidemiology. 2009;169(11):1296–303.
23. Metcalfe K. Cardiac problems in genetic syndromes. Paediatrics and Child Health (United Kingdom) [Internet]. 2018;28(12):574–8. Available from: https://doi.org/10.1016/j.paed.2018.10.005
24. Lee M-Y, Won H-S, Baek JW, Cho J-H, Shim J-Y, Lee P-R, et al. Variety of prenatally diagnosed congenital heart disease in 22q11.2 deletion syndrome. Obstetrics & Gynecology Science. 2014;57(1):11.
25. Doshi-Velez F, Ge Y, Kohane I. Comorbidity clusters in autism spectrum disorders: An electronic health record time-series analysis. Pediatrics. 2014;133(1).
26. Debbané M, Fountain DM, Mutlu AK, Eliez S, Schaer M, Schneider M. Congenital heart disease is associated with reduced cortical and hippocampal volume in patients with 22q11.2 deletion syndrome. Cortex. 2014;57:128–42.
27. Napolitano C, Timothy KW, Bloise R, Priori SG. CACNA1C-Related Disorders. In: M P Adam (Eds) et al. University of Washington, Seattle: GeneReviews; 2006.
28. Boczek NJ, Ye D, Jin F, Tester DJ, Huseby A, Bos JM, et al. Identification and Functional Characterization of a Novel CACNA1C -Mediated Cardiac Disorder Characterized by Prolonged QT Intervals with Hypertrophic Cardiomyopathy, Congenital Heart Defects, and Sudden Cardiac Death. Circulation: Arrhythmia and Electrophysiology. 2015;8(5):1122–32.
29. Pagon RA, Graham JM, Zonana J, Yong SL. Coloboma, congenital heart disease, and choanal atresia with multiple anomalies: CHARGE association. The Journal of Pediatrics. 1981;99(2):223–7.
30. Meisner JK, Martin DM. Congenital heart defects in CHARGE: The molecular role of CHD7 and effects on cardiac phenotype and clinical outcomes. American Journal of Medical Genetics, Part C: Seminars in Medical Genetics. 2020;184(1):81–9.
31. Corsten-Janssen N, Kerstjens-Frederikse WS, du Marchie Sarvaas GJ, Baardman ME, Bakker MK, Bergman JEH, et al. The cardiac phenotype in patients with a CHD7 mutation. Circulation: Cardiovascular Genetics. 2013;6(3):248–54.
32. Blake KD, Prasad C. CHARGE syndrome. Orphanet Journal of Rare Diseases. 2006;1(1):1–8.
33. Morales-Demori R. Congenital heart disease and cardiac procedural outcomes in patients with trisomy 21 and Turner syndrome. Congenital Heart Disease. 2017;12(6):820–7.
34. Acampa M, Guideri F. Cardiac disease and Rett syndrome. Archives of Disease in Childhood. 2006;91(5):440–3.
35. Thapa R, Alvares GA, Zaidi TA, Thomas EE, Hickie IB, Park SH, et al. Reduced heart rate variability in adults with autism spectrum disorder. Autism Research. 2019;12(6):922–30.

36. Bujnakova I, Ondrejka I, Mestanik M, Visnovcova Z, Mestanikova A, Hrtanek I, et al. Autism spectrum disorder is associated with autonomic underarousal. Physiological Research. 2016;65:S673–82.
37. Benevides TW, Lane SJ. A Review of Cardiac Autonomic Measures: Considerations for Examination of Physiological Response in Children with Autism Spectrum Disorder. Journal of Autism and Developmental Disorders. 2013;45(2):560–75.
38. Sheinkopf SJ, Levine TP, McCormick CEB, Puggioni G, Conradt E, Lagasse LL, et al. Developmental trajectories of autonomic functioning in autism from birth to early childhood. Biological Psychology [Internet]. 2019;142(May 2018):13–8. Available from: https://doi.org/10.1016/j.biopsycho.2019.01.003
39. Ornoy A, Liza WF, Ergaz Z. Genetic syndromes, maternal diseases and antenatal factors associated with autism spectrum disorders (ASD). Frontiers in Neuroscience. 2016;10(JUL):1–21.
40. Ciaccio C, Fontana L, Milani D, Tabano S, Miozzo M, Esposito S. Fragile X syndrome: a review of clinical and molecular diagnoses. Italian Journal of Pediatrics. 2017;43(1):1–12.
41. Ellegood J, Crawley JN. Behavioral and Neuroanatomical Phenotypes in Mouse Models of Autism. Neurotherapeutics. 2015;12(3):521–33.
42. Krishnan A, Samtani R, Dhanantwari P, Lee E, Yamada S, Shiota K, et al. A detailed comparison of mouse and human cardiac development. Pediatric Research. 2014;76(6):500–7.
43. The Dutch-Belgian Fragile X Consorthium, Bakker CE, Verheij C, Willemsen R, van der Helm R, Oerlemans F, et al. Fmr1 knockout mice: A model to study fragile X mental retardation. Cell. 1994 Jul 15;78(1):23–33.
44. Horev G, Ellegood J, Lerch JP, Son Y-EE, Muthuswamy L, Vogel H, et al. Dosage-dependent phenotypes in models of 16p11.2 lesions found in autism/ analytic tools; G. 2011;108(41):17076–81.
45. Bozdagi O, Sakurai T, Papapetrou D, Wang X, Dickstein DL, Takahashi N, et al. Haploinsufficiency of the autism-associated Shank3 gene leads to deficits in synaptic function, social interaction, and social communication [Internet]. Vol. 1, Molecular Autism. 2010. Available from: http://www.molecularautism.com/content/1/1/15
46. Zhou Y-Q, Foster FS, Nieman BJ, Davidson L, Chen XJ, Henkelman RM. Comprehensive transthoracic cardiac imaging in mice using ultrasound biomicroscopy with anatomical confirmation by magnetic resonance imaging. Physiol Genomics. 2004;18:232–44.
47. Foster FS, Mehi J, Lukacs M, Hirson D, White C, Chaggares C, et al. A New 15-50 MHz Array-Based Micro-Ultrasound Scanner for Preclinical Imaging. Ultrasound in Medicine and Biology. 2009;35(10):1700–8.
48. R Core Team. R: A language and environment for statistical computing. R Foundation for Statistical Computing. [Internet]. Vienna, Austria; 2019. Available from: https://www.r-project.org/
49. RStudio. RStudio: Integrated Development for R. RStudio, Inc. [Internet]. Boston, MA; 2019. Available from: http://www.rstudio.com/
50. Bürkner PC. brms: An R package for Bayesian multilevel models using Stan. Journal of Statistical Software. 2017;80(1).
51. Bürkner PC. Advanced Bayesian Multilevel Modeling with the R Package brms. The R Journal. 2018;10(July):395–411.
52. Vehtari A, Gabry J, Magnusson M, Yao Y, Bürkner P, Paananen T, et al. loo: Efficient leave-one-out cross-validation and WAIC for Bayesian models. 2020.
53. Gabry J, Goodrich B. rstanarm: Bayesian Applied Regression Modeling via Stan. [Internet]. 2017. Available from: https://mc-stan.org/rstanarm
54. Gabry J, Simpson D, Vehtari A, Betancourt M, Gelman A. Visualization in Bayesian workflow. Journal of the Royal Statistical Society Series A: Statistics in Society. 2019;182(2):389–402.
55. Gelman A. Bayesian data analysis Gelman. Vol. 53, Journal of Chemical Information and Modeling. 2013. 1689–1699.

56. Stan Development Team. Stan Modeling Language Users Guide and Reference Manual. 2017.
57. Vehtari A, Gelman A, Gabry J. Practical Bayesian model evaluation using leave-one-out cross-validation and WAIC. J Stat Comput [Internet]. 2017;27(5):1413–32. Available from: https://arxiv.org/pdf/1507.04544.pdf
58. Makowski D, Ben-Shachar M, Lüdecke D. bayestestR: Describing Effects and their Uncertainty, Existence and Significance within the Bayesian Framework. Journal of Open Source Software. 2019;4(40):1541.
59. Makowski D, Ben-Shachar MS, Chen SHA, Lüdecke D. Indices of Effect Existence and Significance in the Bayesian Framework. Frontiers in Psychology. 2019;10(December):1–14.
60. Storey JD. The positive false discovery rate: A Bayesian interpretation and the q-value. Annals of Statistics. 2003;31(6):2013–35.
61. Timme N, Alford W, Flecker B, Beggs JM, Timme N, Alford W, et al. Synergy, redundancy, and multivariate information measures: an experimentalist's perspective. J Comput Neurosci [Internet]. 2014 [cited 2021 Jun 3];36:119–40. Available from: http://mypage.iu.edu/
62. Banerjee-Basu S, Packer A. SFARI Gene: An evolving database for the autism research community. DMM Disease Models and Mechanisms. 2010;3(3–4):133–5.
63. Wiese C, Grieskamp T, Airik R, Mommersteeg MTM, Gardiwal A, de Gier-De Vries C, et al. Formation of the sinus node head and differentiation of sinus node myocardium are independently regulated by Tbx18 and Tbx3. Circulation Research. 2009;104(3):388–97.
64. Liang D, Xue J, Geng L, Zhou L, Lv B, Zeng Q, et al. Cellular and molecular landscape of mammalian sinoatrial node revealed by single-cell RNA sequencing. Nature Communications. 2021;12(1).
65. Loomes R, Hull L, Mandy WPL. What Is the Male-to-Female Ratio in Autism Spectrum Disorder? A Systematic Review and Meta-Analysis. Journal of the American Academy of Child and Adolescent Psychiatry [Internet]. 2017;56(6):466–74. Available from: http://dx.doi.org/10.1016/j.jaac.2017.03.013
66. Regitz-Zagrosek V, Kararigas G. Mechanistic pathways of sex differences in cardiovascular disease. Physiological Reviews. 2017;97(1):1–37.
67. Lim S, Naisbitt S, Yoon J, Hwang J, Suh P, Sheng M, et al. Characterization of the Shank Family of Synaptic Proteins. Journal of Biological Chemistry. 1999;274(41):29510–8.
68. Cusmano-ozog K, Manning MA, Hoyme HE. 22q13 . 3 Deletion Syndrome : A Recognizable Malformation Syndrome Associated With Marked Speech and Language Delay. American Journal of Medical Genetics. 2007;145(C):393–8.
69. Phelan K, McDermid HE. The 22q13.3 deletion syndrome (Phelan-McDermid syndrome). Molecular Syndromology. 2012;2(3–5):186–201.
70. Man W, Gu J, Wang B, Zhang M, Hu J, Lin J. SHANK3 Co-ordinately Regulates Autophagy and Apoptosis in Myocardial Infarction. Frontiers in Physiology. 2020;11(1082).
71. Santamore WP, Italia LJD. Ventricular Interdependence : Significant Left Ventricular Contributions to Right Ventricular Systolic Function. Progress in Cardiovascular Diseases. 1998;40(4):289–308.
72. Howard LS, Grapsa J, Dawson D, Bellamy M. Echocardiographic assessment of pulmonary hypertension : standard operating procedure. European Respiratory Review. 2012;21(125):239–48.
73. Hart JP, Cabreriza SE, Walsh RF, Printz BF, Blumenthal BF, Park DK, et al. Echocardiographic Analysis of Ventricular Geometry and Function During Repair of Congenital Septal Defects. The Annals of Thoracic Surgery. 2004;77:53–60.
74. Suri RM, Aviernos J, Dearani JA, Mahoney DW, Michelena HI, Schaff H v, et al. Management of less-than-severe mitral regurgitation : should guidelines recommend earlier surgical intervention ? European Journal of Cardio-thoracic Surgery. 2011;40:496–502.
75. Patel H, Desai M, Tuzcu EM, Grif B, Kapadia S. Pulmonary Hypertension in Mitral Regurgitation. Journal of the American Heart Association. 2014;1–9.

76. Scampardonis BG, Yang SSAN, Maranhao V, Goldberg H, Goocn AS. Left Ventricular Abnormalities in Prolapsed Mitral Leaflet Syndrome Review of Eighty-Seven Cases. Circulation. 1973;
77. Tassanakijpanich N, Cohen J, Cohen R, Srivatsa UN, Hagerman RJ. Cardiovascular Problems in the Fragile X Premutation. Frontiers in Genetics. 2020;11(October):1–8.
78. Hempel M, Brugués NR, Wagenstaller J, Lederer G, Weitensteiner A, Seidel H, et al. Microdeletion syndrome 16p11.2-p12.2: Clinical and molecular characterization. American Journal of Medical Genetics, Part A. 2009;149(10):2106–12.
79. Ghebranious N, Giampietro PF, P. Wesbrook F, Rezkalla SH. A Novel Microdeletion at 16p11.2 Harbors Candidate Genes for Aortic Valve Development, Seizure Disorder, and Mild Mental Retardation. American Journal of Medical Geneticsgenetics. 2007;143(A):1462–71.
80. Schussheim AdamE, Diamond JA, Jhang JS, Phillips RA. Midwall Fractional Shortening Is an Independent Predictor of Left Ventriculae Diastolic Dysfunction in Asymptomatic Patients with Systemic Hypertension. American Journal of Cardiology. 1998;82(9):1056–9.
81. Zoccali C, Benedetto FA, Mallamaci F, Tripepi G, Giacone G, Cataliotti A, et al. Prognostic Value of Echocardiographic Indicators of Left Ventricular Systolic Function in Asymptomatic Dialysis Patients. Journal of the American Society of Nephrology. 2004;15(4):1029–37.
82. Cheng A, Nguyen TC, Malinowski M, Daughters GT, Miller DC, Ingels Jr. NB. Heterogeneity of Left Ventricular Wall Thickening Mechanisms. 2009;118(7):713–21.
83. Cotney J, Muhle RA, Sanders SJ, Liu L, Willsey AJ, Niu W, et al. The autism-associated chromatin modifier CHD8 regulates other autism risk genes during human neurodevelopment. Nature Communications. 2015;6(6404).
84. Cohen ED, Tian Y, Morrisey EE. Wnt signaling : an essential regulator of cardiovascular differentiation , morphogenesis and progenitor self-renewal. Development. 2008;135(5):789–98.
85. Hubert F, Payan SM, Rochais F. FGF10 Signaling in Heart Development, Homeostasis, Disease and Repair. Frontiers in Genetics. 2018;9(November):1–7.
86. Nishiyama M, Oshikawa K, Tsukada Y, Nakagawa T, Nakayama KI. CHD8 suppresses p53-mediated apoptosis through histone H1 recruitment during early embryogenesis. 2011;11(2):172–82.
87. Shanks MO, Lund LM, Manni S, Russell M, Mauban JRH, Bond M. Chromodomain Helicase Binding Protein 8 (Chd8) Is a Novel A-Kinase Anchoring Protein Expressed during Rat Cardiac Development. PLoS ONE. 2012;7(10).
88. Batsukh T, Pieper L, Koszucka AM, Velsen N von, Hoyer-fender S, Elbracht M, et al. CHD8 interacts with CHD7 , a protein which is mutated in CHARGE syndrome. Human Molecular Genetics. 2010;19(14):2858–66.
89. Dangel JH. Cardiovascular changes in children with mucopolysaccharide storage diseases and related disorders - clinical and echocardiographic findings in 64 patients. European Journal of Pediatrics. 1998;157:534–8.
90. Nijmeijer SCM, de Bruin-Bon RHACM, Wijburg FA, Kuipers IM. Cardiac disease in mucopolysaccharidosis type III. Journal of Inherited Metabolic Disease. 2019;42:276–85.
91. Marques Ribeiro E, Brusius-facchin AC, Leistner-segal S, Antônio C, Vanessa I. Cardiac disease as the presenting feature of mucopolysaccharidosis type IIIA : A case report. Molecular Genetics and Metabolism Reports [Internet]. 2014;1:422–4. Available from: http://dx.doi.org/10.1016/j.ymgmr.2014.09.003
92. Kivitie-Kallio S, Eronen M, Lipsanen-Nyman M, Marttinen E, Norio R. Cohen syndrome : evaluation of its cardiac , endocrine and radiological features. Clinical Genetics. 1999;56:41–50.
93. Kivitie-kallio S, Norio R. Cohen Syndrome : Essential Features , Natural History , and Heterogeneity. American Journal of Medical Genetics. 2001;102:125–35.
94. Rodrigues JM, Fernandes HD, Caruthers C, Braddock SR, Knutsen AP. Cohen Syndrome : Review of the Literature. 2018;10(9):1–8.

95. Berry-Kravis E, Hipp H, Hunter JE, Saul RA, Tarleton JC, Todd PK. FMR1 Disorders. In: Pagon R, Adam M, Ardinger H, Wallace S, Amemiya A, Bean L, et al., editors. GeneReviews [Internet]. Seattle (WA): GeneReviews; 2019. Available from: http://europepmc.org/article/NBK/NBK1116